SCIENCE & GLOBAL SECURITY
https://doi.org/10.1080/08929882.2026.2756762

Routledge
Taylor & Francis Group

RESEARCH ARTICLE

Check for updates

Assessing the Impact of the Prompt Effect of a High-Altitude Nuclear Explosion on Nonmilitary LEO Satellites

Zhengqing Fang[a] and Igor Morić[b]

[a]Department of Aerospace Engineering, Tsinghua University, Beijing, China; [b]Program on Science and Global Security, Princeton University, Princeton, NJ, USA

ABSTRACT

As the orbital environment becomes increasingly and strategically contested, concerns are growing about the potential consequences of nuclear use in orbit. This paper examines the prompt effects of nuclear detonation on the population of nonmilitary satellites in low Earth orbit, which represent critical infrastructure for civilian and, increasingly, military capabilities. Assuming X-rays dominate the energy output, the lethal radii from the detonation point within which satellite systems would be destroyed were calculated to be approximately 240 km, 760 km, 1700 km, and 2400 km for explosion yields of 10 kt, 100 kt, 500 kt, and 1 Mt, respectively. Detonation coordinates and burst altitudes were varied to identify the maximum number of satellites that would be destroyed across different cases. The simulations show that, out of the 12,334 nonmilitary satellites operational as of November 2025, about 0.2%, 0.7%, 2.7%, and 4.6% of the total number could be permanently disabled for the respective yields, demonstrating a nearly linear scaling relationship between the loss fraction and explosion yield. The effects of a nuclear explosion on future large-scale constellations were also studied. A single 1-Mt detonation could disable up to 4.3% of Starlink's planned, fully deployed 34,396-satellite constellation. Finally, the analysis demonstrates that nuclear weapon states have different degrees of dependence on space-based capabilities and that asymmetries in orbital distributions of constellations could enable a state to optimize detonation parameters that maximize damage to systems on which its adversary is reliant while minimizing collateral damage to its own.

ARTICLE HISTORY
Received 7 January 2026
Accepted 9 September 2026

Introduction

Increasing civilian demand for communication, navigation and Earth observation space-based capabilities, together with decreasing launch costs, technological advancements, and improved manufacturing capacity, has

CONTACT Igor Morić imoric@princeton.edu Program on Science and Global Security, Princeton University, Princeton, NJ, USA.
© 2026 Taylor & Francis Group, LLC

led to a dramatic increase in the number of commercial satellites and satellites operated by civilian organizations in low Earth orbit (LEO), hereafter referred to as "nonmilitary" satellites. While these systems may not be owned or operated by military organizations or defense agencies, they constitute critical infrastructure that can also support military operations.[1] Over the last decade, the total number of active nonmilitary satellites in orbit has increased nearly ninefold, rising from 1,296 in 2014 to 12,334 by November 2025.[2] Around 100,000 satellites are expected to be in orbit by 2030.[3]

This expansion is accompanied by a deepening integration of commercial space assets into military operations, increasingly blurring the boundary between civilian and defense capabilities. Commercial satellite imagery from operators like Maxar, Planet, and ICEYE is now routinely used for military reconnaissance and surveillance of borders and national territory, while communications networks like Starlink provide critical battlefield connectivity.[4] Moreover, commercial operators rely heavily on defense contracts and even develop dedicated military variants like SpaceX's Starshield.

The rapid proliferation of such LEO systems, however, introduces potential security risks in conflict scenarios. Nonmilitary systems are typically unprotected and vulnerable to a range of attack vectors, including cyber operations, uplink and downlink jamming, conventional kinetic anti-satellite weapons, dual-use maneuverable satellites, as well as radiation effects from high-altitude nuclear explosions (HANE).

In February 2024, the U.S. National Security Advisor Jake Sullivan warned that the Russian COSMOS-2553 satellite could be related to a nuclear anti-satellite capability under development.[5] This raised public concerns and drew attention to the potential use of nuclear weapons in outer space and the vulnerability of LEO satellites. While U.S. officials claimed this system could be intended to destroy, blind, or disable other satellites, the Russian Ministry of Defense maintained that the mission of COSMOS-2553 was to study the effects of radiation and charged particles on onboard systems.[6] Since the satellite was placed in a region not typically used by any other spacecraft and with the radiation environment lower than needed to allow accelerated testing of electronics, doubts about its true nature persist.[7]

The destructive capability of nuclear weapons to promptly deny an adversary's space-based capabilities has been long recognized. To understand the military effects of nuclear detonations in space and in the upper atmosphere, the United States and the Soviet Union conducted a series of HANE tests in the 1960s. The most notable event was Starfish Prime, executed in 1962, which involved a 1.4-Mt blast at an altitude of 400 km, generating an artificial aurora that was visible from 900 miles away.[8] Studies indicate that at least 8 satellites suffered damage related to Starfish

Prime, representing roughly one-third of the total 24 satellites that were in orbit at the time or launched in the following weeks. Furthermore, the artificial radiation belt created by the event severely shortened the lifespans of satellites launched in the following months, such as Telstar-1, ultimately leading to their failure.[9]

The widespread disruption caused by this and similar tests galvanized international efforts to establish legal frameworks prohibiting nuclear explosions in space. The 1963 Partial Test Ban Treaty (PTBT) bans nuclear weapons testing in space, while the 1967 Outer Space Treaty (OST) forbids countries from placing "nuclear weapons or any other kinds of weapons of mass destruction" in outer space. The PTBT and the OST have been foundational to maintaining the current peaceful environment: no state has since tested a nuclear weapon in space because the ban serves the interests of every advanced military and national space agency.[10]

Amid worsening geopolitical conditions and increasing tensions between nuclear weapon states, outer space is increasingly becoming the focus of international strategic competition and increased militarization. As most recently made explicit by President Trump's 18 December 2025, Executive Order "Ensuring American Space Superiority," space is the most important strategic domain and achieving superiority is "a measure of national vision and willpower.[11] Countries are developing anti-satellite (ASAT) capabilities, deploying dual-use space-based systems (including maneuverable satellites), and establishing new structures responsible for commanding their space forces. For example, the United States, Russia, China and India have demonstrated direct ascent ASAT capabilities by successfully destroying their own defunct satellites.[12] Additionally, between 2019 and 2021, the United States, France, Japan, the United Kingdom, and Germany have all established Space Commands.[13]

While primarily targeting military adversaries, these capabilities can also be used against nominally commercial systems deployed for military purposes. Recent examples include Russian efforts to jam Starlink systems, alongside with the maneuvering of military satellites to shadow ICEYE's commercial radar assets assisting Ukraine.[14]

However, as satellite constellations become increasingly proliferated, conventional ASAT capabilities or targeted countermeasures may prove insufficient to disable an entire architecture. This limitation has heightened concerns over the potential use of HANE to broadly disrupt or destroy LEO constellations again.[15] In December 2024, the United Nations General Assembly (UNGA) reaffirmed the prohibition of the deployment of weapons of mass destruction in outer space and called for state-parties not to develop nuclear weapons or any other kinds of weapons of mass destruction specifically designed to be placed in orbit around Earth.[16]

A critical need exists to assess the effect of HANE and its potential impact on the current generation of LEO satellites. To date, however, research in this domain remains markedly limited. Most existing studies are largely qualitative, relying on ambiguous damage criteria and neglecting the multifaceted impacts of a nuclear explosion. Quantitative research is particularly scarce because detailed models are often confidential and based on limited experimental results, primarily those derived from events such as Starfish Prime.

Two key reports from the U.S. Defense Threat Reduction Agency (DTRA) have provided valuable insights by systematically analyzing the damage caused by HANE on a sample satellite system. By simulating the faults in electronic components induced by the produced radiation, the reports concluded that while the probability of an individual satellite being threatened by prompt radiation effects is relatively low, LEO satellites are at serious risk of exceeding total-dose limits from trapped radiation. This risk is delayed and not related to distance, as electrons get trapped in magnetic fields, forming radiation belts through which all satellites at certain altitudes will pass.[17] Based on the damage estimate from the DTRA reports, the RAND Corporation published a study in 2025 assessing the prompt effects of space and near-space nuclear detonations on nonmilitary satellites from a HANE detonated at altitudes of 400 km and 30 km, among other scenarios and effects.[18]

However, this study considered an X-ray radiation threshold of 0.4 J/m^2 for satellite systems. According to the 2010 DTRA report by Conrad et al., this level of exposure would only cause reversible, nonpermanent damage (upsets) to a typical non-hardened satellite system. In most cases, the resulting circuit logic errors could then be handled by the system's redundancy and fault tolerance, or, at worst, require only system resets or power-cycling to recover in less than one minute, causing minor capability degradation.[19] In the case of a nuclear attack, such temporary disruption leaves the attacker uncertain whether a target has been neutralized, remains partially functional or can be quickly rebooted and recover full functionality. While the satellite systems would still be exposed to delayed radiation effects, these may take weeks or months to manifest. Therefore, to ensure that critical capabilities—such as early warning systems—remain suppressed throughout the entire attack window, an attacker could require radiation exposure sufficient to cause permanent, irreversible damage.

To assess the strategic impact of a potential HANE to promptly and permanently disable satellites, this paper presents a physical model integrating diverse hardware damage mechanisms induced by a nuclear detonation with detailed orbital mechanics, and examined the effect of a single-HANE-generated prompt radiation on all currently operational nonmilitary LEO satellites, the planned Starlink mega-constellation of

communication satellites, and the PlanetScope constellation of Earth observation satellites at its historical full configuration. By quantifying these impacts, the study also explores how system vulnerabilities can be reduced, such as through hardening, constellation proliferation, or improving operational responsiveness by orbital maneuver, to protect space-based capabilities.

Orbital elements required to uniquely identify a satellite's orbit can be obtained from public catalogs such as Space-Track and CelesTrak. Due to cost constraints, nonmilitary satellites are generally not hardened against the impacts of nuclear weapons; therefore, we assume they have the same vulnerability to HANE. If most of the energy released by HANE is in the form of X-rays, a threshold of 40 J/m^2, derived from an analysis of interaction mechanisms (see Appendix B), was determined as the fluence required to cause permanent damage to nonmilitary satellites.[20]

For the military intelligence and nuclear command and control satellites, some are presumed to be hardened against nuclear attack, and their damage thresholds and probabilities of surviving the detonation are significantly higher.[21] Assessing such assets requires a fundamentally different analytical framework due to specialized shielding and complex survival probabilities. Given that the vast majority of contemporary space-based capabilities rely on unhardened nonmilitary satellites, evaluating their vulnerability to HANE constitutes the primary focus of this research.

The next section details the effects of HANE and the physical model of its interaction with satellites. The following section simulates orbital detonation scenarios for publicly cataloged nonmilitary LEO satellites and constellations and analyzes the results. The discussion then examines the impact of HANE on space-based capabilities and assesses the mutual vulnerability of HANE on satellites. The conclusion summarizes the contributions of this study and provides recommendations. Appendices A–C provide a supplementary overview of delayed effects, damage threshold calculations, and orbital dynamics modeling, respectively.

Modeling the impact of HANE on nonmilitary satellites

Prompt, delayed and atmospheric effects of HANE

HANE is defined as a nuclear detonation above 30 km (19 miles).[22] Its effects can be divided into three categories:[23]

- Prompt effects include high levels of radiation in the form of gamma rays, X-rays, and neutrons.
- Delayed effects include long-term radiation from free electrons trapped in artificial radiation belts, and the potential of a chain reaction from collisions of debris produced by such fragmentation.

- Atmospheric effects include the generation of a ground electromagnetic pulse (EMP) from gamma rays striking atmospheric molecules.

To evaluate the immediate impact of HANE on capabilities provided by nonmilitary satellites, the focus of this study is on the prompt effects. Delayed effects typically take days to months to disable satellites. While their effect on LEO systems would be significant, leading to the degradation of communication and observation capabilities and potentially causing orbital pollution, these would happen gradually and are not likely to provide immediate advantage to the attacker. In addition, simulating delayed effects is very challenging due to the complexity of the physical processes involved and the lack of experimental data. An overview of delayed effects is provided in Appendix A.

Altitude, or height of burst (HOB), is a key factor determining whether the most significant effects of a HANE are experienced by systems in orbit. Atmospheric detonations at 30–100 km generate radiation that is largely absorbed by the Earth's atmosphere, even though it can locally disrupt satellite communications by producing an EMP. The pulse can temporarily impair radio and optical links by ionizing the atmosphere or by directly damaging ground station electronics. However, because the prompt radiation from such lower-altitude bursts is largely absorbed by the atmosphere, its direct impact on orbital assets is minimal and thus excluded from this analysis.[24]

HANE produces high levels of prompt radiation in the form of gamma rays, X-rays and neutrons. If not shielded by Earth, the radiation fluence reaching the satellites is inversely proportional to the square of the distance from the explosion. Most of the energy from HANE is released by X-rays.[25] Assuming that X-rays are uniformly distributed on a spherical surface with radius r, the equation for the X-ray fluence $F_{\text{x-ray}}$ is:

$$F_{\text{x-ray}} = \frac{\eta_{\text{x-ray}} YE}{4\pi r^2} \tag{1}$$

where $\eta_{\text{x-ray}}$ is the fraction of energy converted into X-rays, assumed to be 70% as a lower bound of the typical 70%–80% range; Y is the TNT yield in kilotons (kt); and E is the energy per unit yield, which is 4.184×1012 joules per kt.[26]

Although satellite systems cannot be effectively shielded from neutrons and gamma rays (typically 0.1–10 MeV), their contribution accounts for only about 3% of the total energy generated.[27] Based on the calculation formulas for neutron fluence and gamma-induced total ionizing dose established by Snyder et al., they pose a much lower risk of permanent

damage to satellite subsystems than X-rays (typically 0.1–10 keV) at equivalent distances, and are not considered in the analysis.[28]

The remaining energy from HANE is released as the kinetic energy of fission fragments, as well as fission and fusion fuel. These are ignored in the calculations, since the flux of microscopic particles is relatively small compared to that of X-rays. In addition, as the fission products are typically highly charged heavy ions, their range in aluminum is only about 4 mg/cm^2, equivalent to about 15 µm depth, and would be absorbed by the satellite's outer shell.[29] These effects are ignored in calculations.

Radiation thresholds of satellite subsystems

The ultimate failure of a satellite exposed to HANE results from an electrical, optical, mechanical, or thermal-control malfunction. As described by Conrad et al., the major satellite subsystems most vulnerable to radiation are:[30]

- Power System: solar panel, power management electronics.
- Communication System: antenna, receiver/transmitters.
- Attitude and Orbit Control System.
- Information Processing System: logic elements, memory.
- Thermal Control System: radiator panels, paints, blankets, louvers.
- Surveillance System: passive optical components, optical structural components, spectral imaging, focal plane detectors and processors, information conditioners.

Focusing on the effect of X-rays, which as previously described account for the majority of energy produced by HANE, satellites are primarily affected through three mechanisms:[31]

1. Thermal effects: When X-rays are absorbed, part of that energy is converted to heat, increasing the temperature of the exposed surface. If the energy is absorbed fast enough, the heating can result in melting and spallation, or create a shock wave in the material, causing fractures. This temperature rise can damage materials throughout the satellite. Solar panels, the power source to most satellites, are particularly susceptible to thermal effects.
2. System-generated electromagnetic pulse (SGEMP) effects: The absorption of X-rays in conductors, including metal shielding, can knock electrons from atoms, inducing a high-voltage and electrical current surge. SGEMP primarily threatens the satellite's electronic components.
3. Ionizing effects: Higher energy X-rays can ionize materials, to which semiconductor devices are particularly sensitive. Ionization can

temporarily upset or permanently damage electronics and electronic memory. The specific mechanisms of action are categorized into two types: total-dose effects and dose-rate effects.

Figure 1 summarizes types of damage produced by HANE-generated X-rays (y-axis), as a function of fluence (x-axis; units uniformly converted to J/m^2) on a logarithmic scale. The boxes delineate the range of X-ray fluence thresholds at which each effect first appears. Accounting for uncertainties across satellite models, these intervals represent the damage onset thresholds for typical non-hardened systems, marking the ranges over which damages begin rather than a single arbitrary value. Based on the interaction mechanism, the potential damage to the system was separated into two regions: permanent (irreversible) in pink and temporary (reversible) in blue. The specific calculation details based on publicly available models can be found in Appendix B.

With the assumption that nonmilitary satellites are not specifically hardened against radiation and have no additional shielding, the X-ray fluence required to cause permanent damage was established as an approximate threshold of 40 J/m^2. The threshold comes from the dose-rate ionizing effect of HANE, where the transient burst of X-rays is likely to induce "latch-up", creating a low-impedance path between power and ground

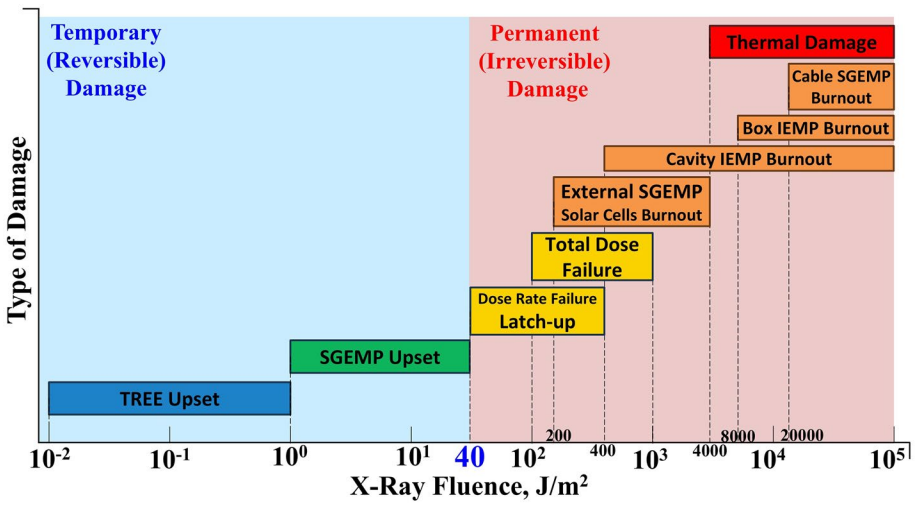


Figure 1. Types of damage experienced by components of a satellite system (y-axis) as a function of X-ray fluence (x-axis). The boxes delineate the possible ranges of X-ray fluence thresholds at which each effect first appears, reflecting physical and design uncertainties (e.g., variations in shielding thickness, component layouts, and semiconductor sensitivity across different satellite models). Higher fluence levels inherently encompass lower-level failure mechanisms. The pink area on the chart includes effects leading to permanent damage, while the light blue area shows reversible and temporary effects. Dashed line at 40 J/m2 shows the minimum X-ray radiation threshold at which the satellite would be rendered permanently damaged.

within CMOS integrated circuits, and resulting in a high-current flow that triggers binary logic state changes, memory erasure, and potentially leads to permanent device failure.[32] For unhardened commercial electronics, latch-up represents the prompt destructive mechanism with the lowest threshold under intense X-ray pulses. An additional sensitivity analysis was performed to assess the impact of the threshold value on the number of satellite losses in the case of nuclear detonation.

Simulating the impact of HANE on nonmilitary LEO satellites

Parameters of HANE and configuration of satellites

The X-ray fluence threshold of 40 J/m^2, defined in the previous section, is used with Equation (1) to determine the maximum lethal distance from a HANE, as a function of the explosion yield. To quantitatively assess how HANE would affect operational nonmilitary LEO satellite systems, the simulation considers the altitude and coordinates of the explosion in relation to orbital positions of tracked satellites, as provided by the CelesTrak and Space-Track public databases.[33] The orbital dynamics model used to calculate satellite positions from TLEs at a given epoch is detailed in Appendix C. When simulating the impact on the Starlink mega-constellation and the PlanetScope constellation, their configuration was determined from publicly available information, as also described in Appendix C.

A time epoch was selected, and HANE coordinates were evaluated over a grid covering the entire LEO space with 0.1° spacing in latitude and longitude and 1 km spacing in altitude to identify the worst-case scenario in which the largest number of satellites would be permanently damaged. In all cases, only satellites with a clear line of sight to the blast were considered. This was determined using the three-dimensional position of each satellite at the time of the explosion, requiring the entire path between the satellite and the blast point to remain above 100 km altitude to avoid shielding by Earth or attenuation by the dense lower atmosphere. All simulations were run on MATLAB 2024b.

HANE altitude and yield. Effects of HANE were simulated above the atmosphere in the LEO region, which is defined as an altitude from 160 km to 2000 km.[34] This is above the upper limit of 100 km where the explosion energy is largely absorbed by the Earth's atmosphere, as discussed above. The lower bound of 160 km was selected because active satellites operate almost exclusively above this height due to intense atmospheric drag; any object below 160 km is typically in a state of rapid decay and imminent reentry.

When choosing the yield of the nuclear detonation, states are likely to select and modify already stockpiled weapons, as was the case with the

Table 1. Overview of deployed U.S., Chinese and Russian nuclear delivery vehicles and warhead yields.

	United States	China	Russia
SRBMs	—	—	Iskander-M
IRBMs	—	DF-26, 5-10 kt	RS-26 3-6 warheads of 10-100 kt
ICBMs	Minuteman III, W78: 335 kt W87: 300 kt	DF-41/DF-5C, Single warhead 1 Mt, or 10 warheads of 20/90/150 kt	RS-24 / SS-18 Mod 6 3 warheads of 100 kt; SS-18 Mod 6 (R-36M2), 10 warheads of 500–750 kt
SLBMs	Trident II D-5, W76/W76-1: 90–100 kt W76-2: 5–7 kt W88: 475 kt	JL-3, 10-100 kt	RSM-56 6 warheads of 100 kt

1962 Starfish Prime test which deployed an existing W49 warhead.[35] To represent realistic threat scenarios, the simulated nuclear yields are chosen to reflect currently deployed warheads and delivery vehicles in the U.S., Russian, and Chinese arsenals (see Table 1).[36]

HANE could be deployed by nuclear-armed co-orbital satellites or launched to orbit with ballistic missiles. A useful rule of thumb is that a missile that can launch a given payload to a maximum range of R on Earth, can launch that same payload to an orbital altitude of roughly $R/2$.[37] Therefore, for targets in LEO, short- or intermediate-range ballistic missiles (SRBMs/IRBMs) can be employed. For higher altitudes and greater distances, intercontinental ballistic missiles (ICBMs) and longer-range submarine-launched ballistic missiles (SLBMs) could be used.

In the simulation scenarios, four representative yield values were selected for the HANE simulation:

- 1 Mt warhead represents the most powerful currently deployed nuclear weapon. This includes the U.S. 1.2 Mt B83.[38] China is also developing a warhead for the DF-5C ICBM.[39] The Starfish Prime test was also in the Mt range, and existing information on the effects of orbital nuclear detonations is likely based on this experimental data.
- 500 kt warhead was chosen to represent the yield of warheads deployed on most land-based ICBMs, such as Russia's SS-18 Mod 6, which carries warheads with a yield of 500–750 kt, and the U.S. Minuteman, which carries warheads with a yield of 300–335 kt.
- 100 kt warhead was selected to represent the yield of most warheads carried by SLBMs, including the U.S. Trident II D-5, Chinese JL-3, and the Russian Bulava.
- 10 kt warhead represents low-yield nuclear weapons carried by the Chinese DF-26, the Russian Iskander-M, and the U.S. SLBM warhead W76-2.

Configuration of nonmilitary LEO satellites. To assess the impact of HANE on nonmilitary LEO satellites, an aggregated payload population of all tracked systems was constructed. Two-Line Element Sets (TLEs) were retrieved from the CelesTrak database, while country affiliations were taken from the Space-Track website.[40]

At the selected date of 2025-11-01T00:00:00Z, there were 13,139 active satellites in orbit, of which 12,334 were in LEO. Since Starlink dominates the LEO population, 77% of all on-orbit satellites were affiliated to the United States. Note that in the database CIS (Commonwealth of Independent States) is the official designator for Russian satellites and this acronym is used accordingly in this paper.

Three different scenarios were simulated: Scenario 1 evaluates the worst-case impact of a single HANE on the aggregated payload population of all nonmilitary LEO satellites as of November 2025; Scenario 2 considers the impact of a HANE on the future Starlink mega-constellation; and Scenario 3 analyzes the impact on the PlanetScope constellation at its historical full configuration.

Starlink is a satellite constellation providing internet access to 150 countries, owned by SpaceX.[41] As of 31 October 2025, 10,213 Starlink satellites have been launched, with 8,821 operational.[42] According to documents SpaceX submitted to the Federal Communications Commission (FCC), Starlink plans to launch a total of 34,396 satellites, including 4,408 Gen1 and 29,988 Gen2 satellites.[43] The parameters of the proposed mega-constellation, under an assumed Walker-Delta configuration for each layer, are described in Appendix C.

PlanetScope is an Earth observation constellation, operated by Planet, consisting of multiple launches of groups of Flock satellites, which are continuously replenished.[44] They provide a high-frequency view of the entire land surface of the Earth, with ~4-meter resolution. As of November 2025, 498 satellites have been launched, with 92 operational. Additionally, Planet also operates the SkySat constellation of 21 satellites.

The Planet constellation is currently undergoing an upgrade, and its configuration is incomplete at the time of this study. Therefore, the time epoch at 2022-03-01T00:00:00Z was selected for this simulation scenario, which is a time epoch when the Planet constellation comprised the full configuration of 375 satellites (including 354 Flock/Dove satellites and 21 SkySat satellites). This constellation is described in more detail in Appendix C. Note that this sample does not include Planet's new Pelican and Tanager satellites, which were deployed after the selected date to replace the SkySat fleet and expand into hyperspectral capabilities.[45]

Simulation results

For Scenario 1 (impact of HANE on the aggregated payload population of nonmilitary satellites), the time epoch 2025-11-01T00:00:00Z was

selected for the detonation, and its orbital position was optimized to inflict maximum damage. Table 2 shows the number and percentage of destroyed systems for different detonation yields, as well as an overview of the number of systems destroyed per country affiliation.

Using Equation (1) and by considering $F_{\text{X-ray}} = 40\,\text{J/m}^2$ as the threshold at which nonmilitary satellites are permanently damaged (from "latch-up," as described earlier), the orbital destructive radii r of 241 km, 763 km, 1,707 km, 2,413 km were calculated for HANE yields $Y = 10$ kt, $Y = 100$ kt, $Y = 500$ kt, and $Y = 1$ Mt, respectively.

The results of the simulation show that out of the 12,334 LEO satellites, HANE with yields $Y = 10$ kt, 100 kt, 500 kt, and 1 Mt would in the worst-case scenario destroy about 19, 83, 331, and 567 satellites, corresponding to approximately 0.2%, 0.7%, 2.7%, and 4.6% of the total number of nonmilitary satellites.

The destructive effects for different yields are illustrated in Figure 2. The Earth is represented as a superimposed sphere with a latitude-longitude grid. The LEO region, spanning altitudes from 160 to 2000 km, is represented by spherical shells (in cyan). The optimized location of the HANE that would destroy the largest number of satellites at the selected time epoch is shown with a red pentagram shape. The orange hemisphere around the blast center describes the destructive radius, while the destroyed satellites are highlighted with yellow dots.

In addition, a nearly linear scaling is observed between the HANE yield and the resulting satellite losses ($R^2 = 0.9914$) for the $F_{\text{X-ray}} = 40\,\text{J/m}^2$ threshold, as shown in Figure 3. Furthermore, to understand the impact of the threshold on the potential satellite losses, a sensitivity analysis was conducted by simulating with the threshold adjusted by ±20%. These variations are depicted as red and green lines in Figure 3. The specific values for satellite losses corresponding to yields of 10 kt, 100 kt, 500 kt, and 1 Mt are annotated in the figure.

Table 2. The altitude and location of HANE (10 kt, 100 kt, 500 kt and 1 Mt yields) permanently damaging the maximum number of nonmilitary satellites (with country affiliation) for time epoch 2025-11-01T00:00:00Z.

Yield	Max Damage Detonation Position	Max Destroyed Satellite Number	Satellites Destroyed of Each Country		
			U.S.	PRC	CIS
10 kt	168.1°W, 52.7°S, 543 km	19 (0.2%)	15 (0.2%)	2 (0.2%)	0 (0.0%)
100 kt	153.3°W, 39.4°N, 525 km	83 (0.7%)	63 (0.7%)	8 (0.8%)	1 (0.6%)
500 kt	171.2°W, 44.6°S, 344 km	331 (2.7%)	267 (2.8%)	20 (2.0%)	3 (1.8%)
1 Mt	176.3°W, 40.2°S, 170 km	567 (4.6%)	458 (4.8%)	36 (3.6%)	7 (4.3%)

Shown are also the total number of destroyed satellites, and the number and percentage of the total nonmilitary satellites destroyed operated from the United States (U.S.), China (PRC) and Russia (CIS).

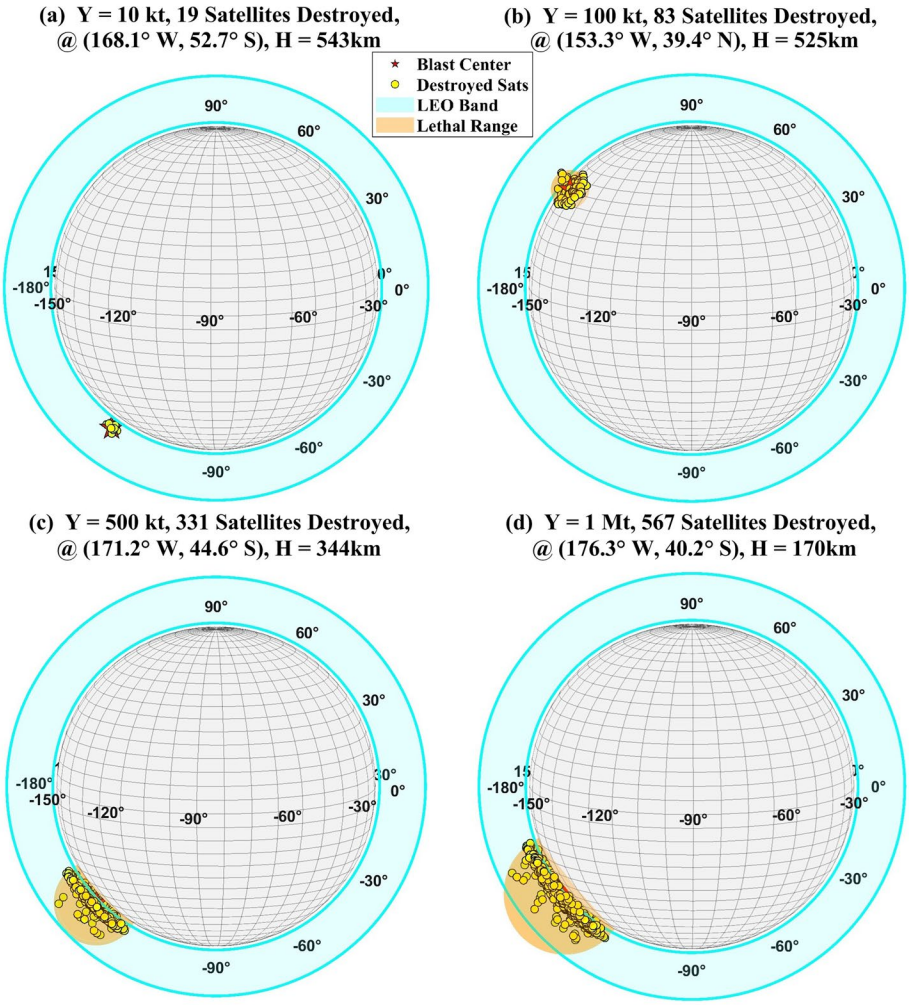


Figure 2. The HANE location and height of burst were optimized to destroy the maximum number of on-orbit nonmilitary LEO satellites for different yields: 10 kt, 100 kt, 500 kt and 1 Mt, in the selected time epoch 2025-11-01T00:00:00Z. The orange sphere represents the region covered by the HANE destructive radius. For the 10 kt detonation scenario shown in (a), the destructive radius of the explosion is too small to be visible at this scale.

The results shown here indicate fewer satellite losses than those presented in the RAND report, which suggested that a 15 kt detonation at 400 km would place approximately 4% of the LEO satellite population at risk from prompt radiation, while a detonation of 110 kt would place 20% at risk.[46] In our model, an equivalent 15 kt detonation at 400 km would destroy approximately 0.2% of satellites, while a 110 kt detonation would destroy 0.7%. This disparity arises because this study adopts an X-ray fluence threshold of 40 J/m^2 strictly for permanent damage, whereas the RAND report uses 0.4 J/m^2 for temporary, reversible circuit upset.

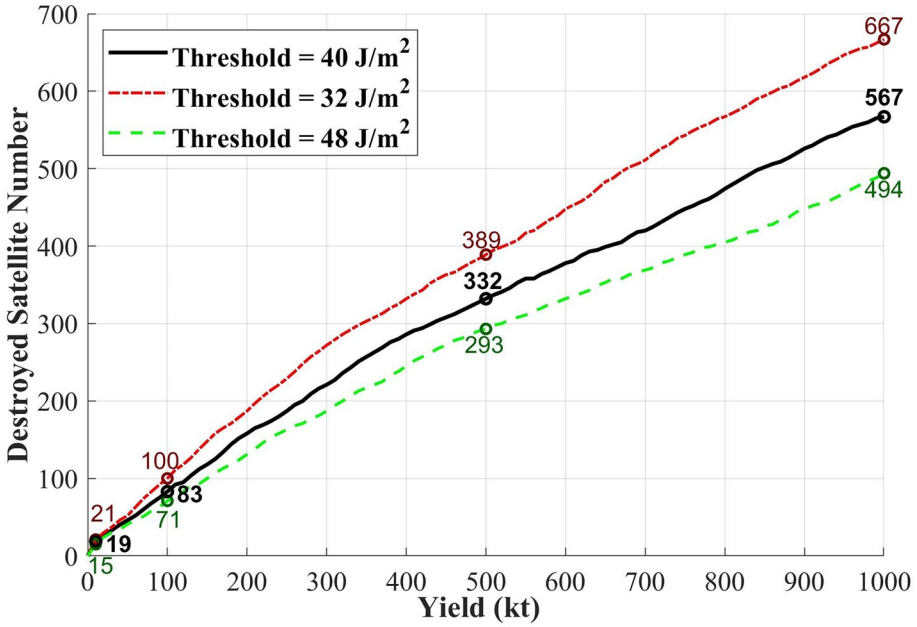


Figure 3. Relationship between HANE yield and the maximum number of destroyed nonmilitary LEO satellites in scenario 1. The simulation was performed at 10 kt intervals, with a maximum value at 1 Mt. The black line represents the baseline scenario (damage threshold of 40 J/m^2), exhibiting strong linearity (R^2 = 0.9914). To illustrate the sensitivity of the selected threshold, the relationship was also examined with a ± 20% variation in the threshold (seen in green and red lines, with the optimal detonation location re-calculated for each data point). Numerical results for 10 kt, 100 kt, 500 kt and 1 Mt are highlighted.

The effects of HANE were also examined for Scenario 2 (the proposed Starlink mega-constellation) and Scenario 3 (the PlanetScope constellation at its historical full configuration). As in Scenario 1, using the 40 J/m^2 X-ray fluence threshold, the yields, detonation coordinates and altitude were varied to obtain the worst-case scenario with the maximum number of systems destroyed.

As Table 3 shows, a 1 Mt HANE at an altitude of 160 km could destroy about 1,479 satellites of the future Starlink mega-constellation (up to 4.3% of the total). Note that this number is 2.6 times larger than the maximum number of systems that a HANE with equivalent yield could destroy today, closely tracking the 2.8-fold ratio of the future Starlink population to the current total LEO population, and confirming that damage scales proportionally with population size under a fixed yield and a uniform spatial distribution. This risk will further compound as other planned constellations, including Amazon's Kuiper (~5,100) and China's Xingwang (12,992) and Qianfan (~15,000), continue to saturate LEO.[47]

On the other hand, a detonation with the same yield at an altitude of 184 km could in the worst case destroy 49 Planet satellites (about 13.1% of the total constellation at maximum size). The impact of HANE on the

Table 3. Maximum number and percentage of destroyed systems of the proposed starlink mega-constellation and planet constellation at its maximum historical size, for different HANE yields.

	Max Destroyed Satellite Data (planned Starlink)		Max Destroyed Satellite Data (full configuration Planet)	
Yield	Max Damage Detonation Position	Number / Percentage	Max Damage Detonation Position	Number / Percentage
10 kt	0.4°W, 0.4°S, 407 km	29 (0.1%)	24.5°W, 81.6°N, 482 km	9 (2.4%)
100 kt	179.7°W, 35.4°N, 371 km	179 (0.5%)	42.1°W, 51.2°N, 298 km	20 (5.3%)
500 kt	110.8°W, 40.1°S, 224 km	799 (2.3%)	43.7°W, 42.1°N, 353 km	39 (10.4%)
1 Mt	179.2°W, 36.0°S, 160 km	1479 (4.3%)	127.9°E, 5.2°S, 184 km	49 (13.1%)

Table also shows the location of the detonation causing most damage for the selected time epochs.

Planet constellation is several times greater than that on Starlink. This is because Starlink utilizes an assumed Walker-Delta configuration, where satellites are distributed more uniformly. In contrast, Planet satellites are mostly concentrated in Sun-synchronous orbits (SSO) at 450–600 km altitudes with inclinations of 97°–98°.

Discussion

Relative Vulnerability of U.S., Chinese and Russian Nonmilitary Satellites to HANE

As shown in Table 2, a single HANE could destroy a large number of satellites operated from different countries. A common hypothesis exists in the literature that it would not make sense for a nuclear weapon state to detonate a warhead in space targeting its adversaries because it would equally damage or destroy its own satellites.[48] Here, the question of whether HANE harms all sides equally is examined by simulating scenarios maximizing the number of nonmilitary LEO systems that could be destroyed by the United States, China or Russia, while minimizing collateral damage they would each sustain.

The United States and China possess the highest number of operational LEO satellites and have the greatest reliance on these systems for military, economic and civilian functions. Considering only nonmilitary LEO satellites, companies and organizations from the United States and China operate 9,535 and 1,007 satellites, respectively, while only 163 are operated by Russia. While most of these satellites provide space-based capabilities that are shared internationally in times of peace (such as communication or observation), in times of conflict, open access faces significant risk of restriction as commercial systems could be folded into national capabilities to serve exclusive state interests.[49] In the case of nuclear war, the attacking country may detonate an orbital nuclear explosion by optimizing the coordinates (primarily

latitude), altitude, and yield to exploit the differences in orbital distributions of satellite constellations. For example, a high-latitude HANE will have a limited impact on low-inclination satellites. The fundamental reason latitude is such an important parameter impacting how much damage HANE would inflict is the inclination distribution of different satellites. The latitude of any point on a satellite's trajectory is always less than or equal to its orbital inclination i. Based on this geometric relation, for a HANE at latitude φ and altitude H with a destructive radius r, satellites in orbits with an inclination less than a specific threshold $i_{(\varphi,\ H,\ r)}$ will not be affected by prompt radiation (R_E is the radius of the Earth):

$$i_{(\varphi,H,r)} = \varphi - \sin^{-1}\left(\frac{r}{R_E + H}\right) \tag{2}$$

As shown in Figure 4, over 80% of the U.S. satellites are at an inclination from 40° to 60°, with more than 7,000 Starlink satellites in the 33°–53.2° orbits comprising over 70% of the national total. Meanwhile, over 60% of Chinese and over 75% of Russian satellites have inclinations between 80°–100°. Therefore, the United States could choose a high-latitude HANE, while China or Russia could select mid-to-low latitude regions to reduce their own losses while increasing the adversary's. This strategy remains effective despite high-inclination satellites periodically traversing mid-to-low latitude regions, as the resulting self-inflicted damage is

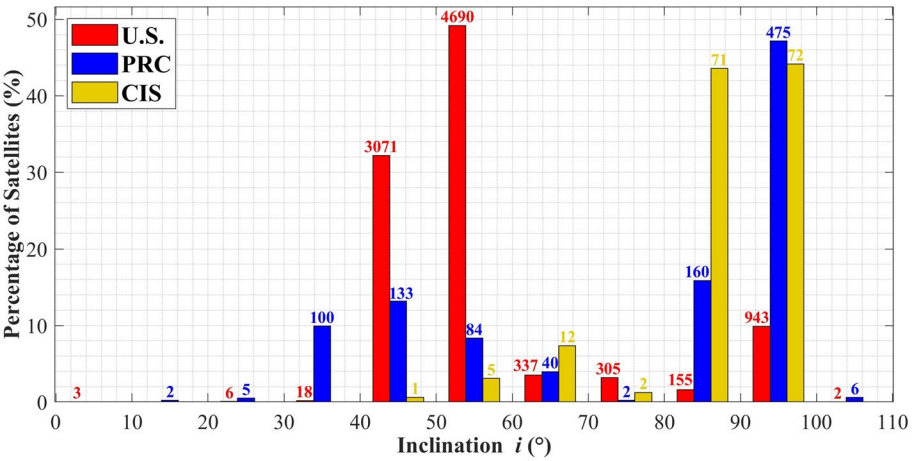


Figure 4. Histogram of orbital inclination i distributions for operational nonmilitary LEO satellites of the U.S., China (PRC), and Russia (CIS) with each interval spanning 10°, based on data from CelesTrak and Space-Track. The y-axis represents the percentage of satellites in the inclination range relative to the total number of satellites in each country, with the absolute number of satellites labeled on each bar. U.S. satellites are predominantly mid-to-low inclination, while Chinese and Russian satellites are predominantly high-inclination.

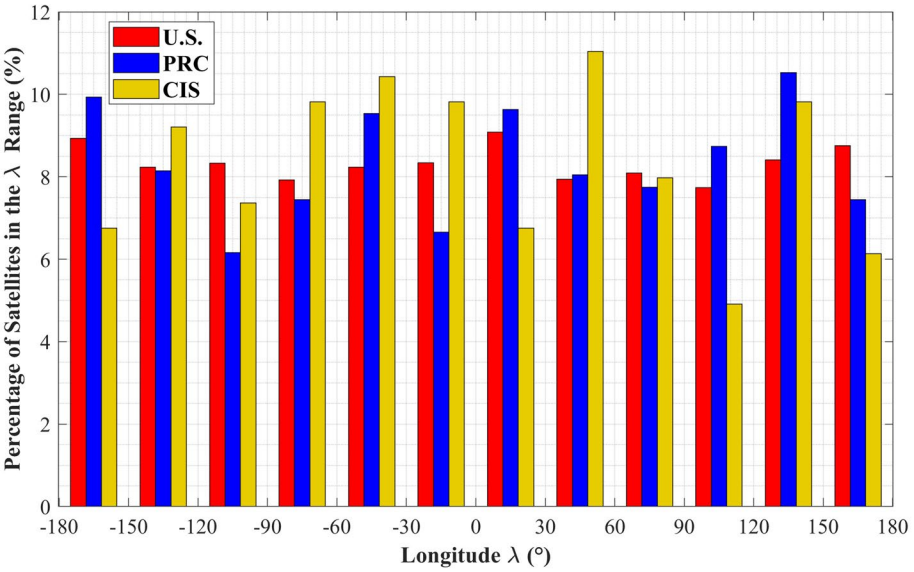


Figure 5. Histogram of longitude λ distributions for operational nonmilitary LEO satellites of the U.S., China (PRC), and Russia (CIS) with each interval spanning 30°, based on data from CelesTrak and Space-Track. The distributions exhibit a near-uniform spread across all longitudes for all three nations.

manageable compared to the disproportionate impact on the adversary's concentrated satellites.

The relative vulnerability of U.S., Chinese and Russian nonmilitary LEO systems from HANE prompt effects was more closely examined with a simulation varying the latitude of the orbital explosion. Since the satellites of all three nations exhibit a uniform longitudinal distribution (Figure 5), a representative longitudinal plane is chosen for this relative vulnerability analysis. Without loss of generality, using the same satellite orbital data as in Scenario 1, the HANE longitude is set to 0°, while the latitude is varied from −90° to 90° with 0.1° spacing. The HOB was set to an altitude of 400 km, and the impact of HANE was simulated for two yields: Y = 100 kt and 1 Mt.

Figure 6 shows the results of the analysis. The losses for the United States (U.S.), China (PRC), and Russia (CIS) are presented as the percentage of each country's total satellite systems that would be destroyed (y-axis) as a function of latitude φ (x-axis) of the detonation. Latitudes with the maximum difference in the percentage of satellites destroyed between two countries are annotated with double arrows on each figure. These are orbital locations at which the country detonating the warhead could inflict maximum damage to the target country, while minimizing its losses.

As seen in (a), it is possible for China, through a single 100 kt HANE, to destroy about 41 U.S. nonmilitary satellites (approximately 0.4% of the total number), while itself incurring zero losses (detonation at latitude

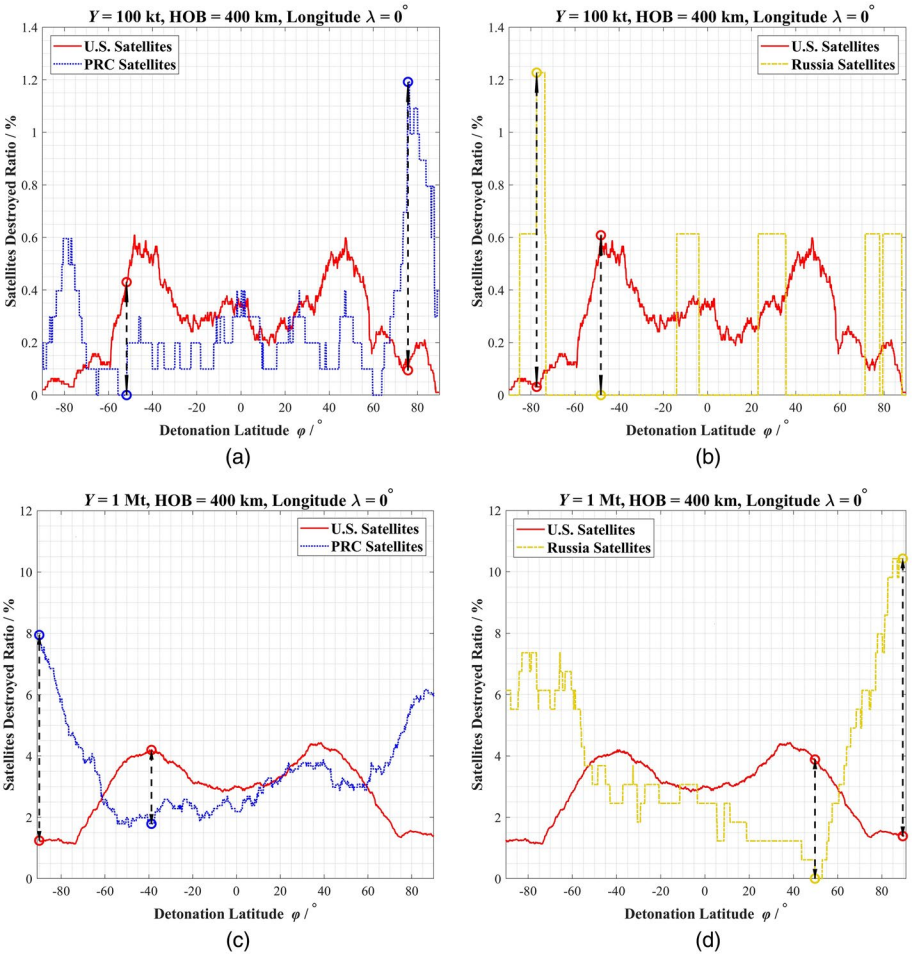


Figure 6. Results of the simulation showing the percentage of the U.S., Chinese and Russian satellite systems destroyed (y-axis) as a function of the orbital detonation latitude (x-axis) at a fixed HOB of 400 km. Top images show the difference between the U.S. and Chinese (PRC) satellites destroyed (left), and the difference between U.S. and Russian satellites destroyed (right) for a detonation with a yield of 100 kt. Bottom images show the same for a detonation with a yield of 1 Mt. Vertical black dashed double-headed arrows on each image show the detonation latitude with the greatest difference of satellites destroyed between two sides, indicating optimum latitudes for attack.

51.8°S). As seen in (b), Russia could, with zero losses, detonate a HANE at latitude 48.3°S and destroy about 58 U.S. satellites (approximately 0.6% of the total number).

In the case of 1 Mt HANE, the United States and China would both experience some level of damage to their nonmilitary fleets, no matter the orbital location of the explosion. In regions above 70°N and below 70°S latitude, China would have greater satellite losses than the United States, while in the mid-low latitudes (20°–60°), the United States would incur greater losses. Specifically, China could detonate HANE at latitude

38.8°S, destroying 400 U.S. satellites or 4.2% of the total, at a minimum cost of 1.8% of its own fleet. Conversely, the United States could detonate a HANE at latitude 90°S and destroy 80 Chinese satellites or 7.9% of the total, at the cost of 1.2% of its fleet. As shown in (d), because Russia has a much smaller number of satellites with a lower distribution density, in the worst-case scenario for the United States, a 1 Mt HANE detonated at latitudes between 50°N to 53°N would destroy 370 U.S. satellites or 3.9% of the total, without any Russian losses.

The findings from this study are illustrative: with higher yields and multiple carefully positioned orbital detonations, an attacker could further amplify the asymmetry in satellite distribution and numbers, inflicting disproportionately greater damage on the adversary's constellations. While the increasing reliance of U.S. and China on space-based capabilities implies a degree of mutual vulnerability, discouraging the use of weapons in space, this is not the case for Russia.[50]

In general, in the short-term, a HANE will cause equivalent damage to both the attacker and the target only if the following two conditions are simultaneously met: (1) the HANE yield is sufficiently large; (2) both sides possess a large number of uniformly distributed satellites.

In the longer term, satellites of all countries are exposed to delayed effects of HANE. After the detonation, some of the generated electrons would remain trapped in radiation belts, damaging all orbital satellites with each pass through, erasing immediate advantages gained by exploiting the different orbital distributions of each state's satellites.[51]

Increasing resilience and robustness of space systems against HANE

An orbital nuclear detonation would inevitably lead to a degradation of space-based capabilities. For example, if a significant number of telecommunication satellites were impacted by HANE, the immediate effect would be a decrease in the service coverage area near the detonation at the time of the event. Subsequently this results in coverage gaps that propagate globally along the orbital paths of the affected satellites, causing users worldwide to experience some level of signal weakening or interruption, as well as reduced throughput and increased signal latency.

One mitigation strategy to limit the impact of HANE on capabilities provided by nonmilitary satellites is to implement hardening of the satellite subsystems, reducing their vulnerability by raising the damage thresholds to HANE-generated radiation. For example, simple shielding can significantly decrease the lethal radius of orbital detonations and enhance the lifetime of a satellite when exposed to conditions of increased radiation. Research indicates that for Planet Flock satellites in a 450 km SSO, increasing the aluminum shielding thickness from 0.25 mm to 0.50 mm would

reduce the total ionizing dose (TID) accumulation in electronic components by more than half.[52] At a greater overall system cost and increased weight, satellite operators also have the option to use radiation-resistant materials and make design choices decreasing the overall system vulnerability.

In addition, modern satellite constellations have evolved from traditional static models, which featured fixed orbits and were independently operated. Today, constellations such as Starlink and PlanetScope already possess self-organizing, responsive, and reconfiguration capabilities, with powerful algorithms capable of managing huge amounts of data, enhancing the utilization efficiency of the constellation.[53]

To reduce degradation of service, future Earth observation mega-constellations could improve operational responsiveness by maneuvering to adjust satellite orbits and constellation configurations.[54] Communication constellations could enhance data transmission and anti-jamming capabilities through inter-satellite links (ISLs) connection and other strategies.[55] For example, one study indicates that a 588-satellite communication constellation can maintain good performance with virtually unchanged communication latency even after up to 25% of the satellites fail.[56]

Conclusions

This paper provides an assessment of the potential impact of a single orbital nuclear detonation on nonmilitary LEO satellites, which are typically not shielded and not protected against the radiation that would be generated. The analysis integrates physical damage mechanisms with detailed orbital mechanics of all currently operational LEO satellites, the proposed Starlink mega-constellation once it is assembled, and the largest Earth observation constellation PlanetScope at its full historical configuration.

The number of satellites impacted depends on their distance from a HANE, and the yield of the explosion. The primary prompt destructive mechanism is through X-ray radiation, which causes damage to a satellite system through thermal, SGEMP, and ionizing effects. A threshold of 40 J/m^2 was determined as the X-ray fluence required to cause irreversible system failure from "latch-up", where the generated current leads to device failure. While the RAND report adopts a lower threshold (0.4 J/m^2) for serious, though not necessarily permanent, damage, this paper uses a higher threshold corresponding to a high probability of permanent, irreversible hardware failure. Temporary upsets can often be cleared in under a minute and therefore do not ensure sustained denial, while delayed effects may take weeks or months to manifest, too slowly to provide immediate military advantage. This could be an important distinction for a potential attacker aiming to detonate a nuclear weapon in LEO.

HANE was simulated with a set of yields Y selected to represent warheads currently present in the arsenals of the United States, China and Russia. The orbital detonation coordinates (longitude λ, latitude φ, and altitude H) were varied to obtain worse-case scenarios with a maximum number of satellites damaged for the three cases.

Key results indicate that in the worst-case scenario, a single 1-Mt HANE would permanently disable approximately 4.6% of all on-orbit LEO nonmilitary satellites, 4.3% of the Starlink mega-constellation, and 13.1% of Planet at historical full configuration, while the lowest 10 kt yield could permanently disable up to 0.2% of all nonmilitary satellites, 0.1% of the Starlink mega-constellation, and 2.4% of the Planet constellation at maximum size.

A 15 kt explosion at 400 km would destroy up to 0.2% of all LEO satellites, while a 110 kt explosion would destroy up to 0.7%. Since this paper uses a higher damage threshold, the resulting estimate of destroyed satellites is considerably lower than in the equivalent scenario as described in the report produced by the RAND Corporation.

According to ESA, with the continued growth of demand for space-based capabilities, the number of on-orbit satellites may increase 8- to 10-fold within the decade, reaching 100,000.[57] As demonstrated by the simulations involving an expanded and completed Starlink mega-constellation, a denser LEO population will further increase vulnerability to a HANE. The number of Starlink satellites potentially destroyed with a 1 Mt detonation would be nearly three times the number of all current nonmilitary satellites.

Detonation latitudes were varied to examine the differences in the impact of HANE on satellite fleets operated from the United States, China and Russia. Because these have different orbital distributions, it was shown that it is possible for the attacker to effectively exploit the difference and optimize the location of a HANE to selectively target the adversary's satellites while minimizing collateral damage to its own systems.

The findings show that the supposition that HANE harms the attacker as much as the target only holds true if the yield of the explosion is sufficiently large, and all sides possess a large number of satellites and are equally reliant on space-based capabilities. While the space competition between the United States and China is accelerating, the use of nuclear weapons in orbit would significantly endanger the critical space-based capabilities of both countries, encouraging mutual restraint and potentially opening the window for cooperation. This may not be the case for Russia, which has a much smaller number of operating space systems and smaller immediate ambitions for outer space expansion. Ultimately, the optimization of such attacks must also account for critical constraints, including

the mitigation of terrestrial collateral damage and limitations tied to the attacker's geographic reach and detonation timing.

What can satellite operators do to decrease the vulnerability of their systems, and protect them against conditions of increased radiation?

The damage caused by HANE would inevitably lead to a degradation in space-based capabilities. However, even if a certain percentage of satellites are destroyed by HANE, modern constellations can still maintain at least partial operational capability through inherent resilience (e.g., inter-satellite links, reconfiguration, etc.) and rapid replenishment of new satellites. As discussed in the preceding section, other mitigating strategies include hardening satellite subsystems, which decrease the lethal radius from orbital detonations. This involves implementing moderate levels of shielding, making design choices that prioritize redundancy, and choosing radiation-resistant materials and components.

What should states do to ensure their space-based capabilities are protected, and that space is used for peaceful purposes and is free of nuclear weapons?

As a priority, states need to re-affirm the core principles enshrined in the OST and work together to stop the ongoing militarization of space, strengthening the norms against placement of nuclear weapons in space. The OST by itself does not guarantee the prevention of an outer space arms race, since it leaves significant gaps regarding the deployment and testing of conventional and nuclear weapons. It also lacks verification and enforcement mechanisms and was not designed to address many of today's dual-use and emerging space technologies.

Relevant efforts could be pursued within frameworks such as the Prevention of an Arms Race in Outer Space (PAROS), which seeks to close loopholes present in the OST and prevent any nation from placing objects carrying any type of weapon into orbit and threatening to use force against objects in outer space, thereby legally encompassing a prohibition on engagements launched from land-based platforms.[58] This treaty advocates dispute resolution through negotiation and cooperation and has been regularly reaffirmed through annual resolutions passed by the UNGA. The core of achieving this objective lies in developing modern verification mechanisms, including on-orbit inspections.[59] These mechanisms should also incorporate shared space situational awareness data and cooperative monitoring protocols.[60]

Notes

1. For example, internet connectivity and communication capabilities provided by Starlink have been crucial for military operations in Ukraine. Charlie Metcalfe, "On the ground in Ukraine's largest Starlink repair shop," 21 August 2025,

https://www.technologyreview.com/2025/08/21/1122035/ukraines-largest-starlink-repair-shop; Companies such as Planet and Maxar are providing data for U.S. intelligence, defense and federal civil agencies. Sandra Erwin, SpaceNews, "BlackSky, Maxar, Planet win 10-year NRO contracts for satellite imagery," 25 May 2022, https://spacenews.com/blacksky-maxar-planet-win-10-year-nro-contracts-for-satellite-imagery.

2. CelesTrak, "NORAD GP Element Sets Current Data," https://celestrak.org/NORAD/elements/gp.php?GROUP=active&FORMAT=tle.
3. Estimation given by European Space Agency (ESA), "Around 100,000 satellites are expected to be in orbit by 2030," 1 April 2025, https://www.esa.int/ESA_Multimedia/Sets/Space_Debris_Is_it_a_Crisis/(result_type)/images.
4. Kari A. Bingen, "Extending the Battlespace to Space," 16 September 2025, *Center for Strategic and International Studies*, https://www.csis.org/analysis/chapter-8-extending-battlespace-space.
5. Daryl G. Kimball, "U.S. Warns of New Russian ASAT Program," Arms Control Association, March 2024, https://www.armscontrol.org/act/2024-03/news/us-warns-new-russian-asat-program.
6. Bart Hendrickx, "Russian research on space nukes and alternative counterspace weapons (part 1)," *The Space Review*, 13 May 2024, https://www.thespacereview.com/article/4793/1.
7. Victoria Samson, Seth Walton, and Kathleen Brett, "FAQ: What We Know About Russia's Alleged Nuclear Anti-Satellite Weapon," *Secure World Foundation*, 26 June 2024, https://www.swfound.org/publications-and-reports/faq-what-we-know-about-russias-alleged-nuclear-anti-satellite-weapon .
8. Liz Boatman, "Sixty Years After, Physicists Model Electromagnetic Pulse of a Once-Secret Nuclear Test," *APS News*, 10 November 2022, https://www.aps.org/apsnews/2022/11/electromagnetic-pulse.
9. See Defense Threat Reduction Agency, Edward E. Conrad et al., "Collateral Damage to Satellites from an EMP Attack," DTRA-IR-10-22, Fort Belvoir, VA, August 2010, 11–13, https://apps.dtic.mil/sti/tr/pdf/ADA531197.pdf.
10. Aaron Boley and Michael Byers, "Anti-satellite weapon tests to disrupt large satellite constellations," *Nature Astronomy* 8 (2024): 10–12.
11. The White House, "Ensuring American Space Superiority," 18 December 2025, https://www.whitehouse.gov/presidential-actions/2025/12/ensuring-american-space-superiority/.
12. Ritu S. Lauer, "When States Test Their Anti-Satellite Weapons," *Astropolitics* 20 (2022): 1–26.
13. Qisong He, "Space Arms Control or Space Behavior Control? The Competition between American and Chinese Ideas of an International Space Order," *Pacific Focus* 38 (2023): 26–51.
14. See Max Hunder, "Russia tries to jam Musk's Starlink systems to counter Ukrainian drones," *Reuters*, 8 July 2026, https://www.reuters.com/business/aerospace-defense/russia-tries-jam-musks-starlink-systems-counter-ukrainian-drones-2026-07-08/; Juliana Suess, "Checkmate? Russian Orbital Manoeuvring Threatens Ukraine's Space Capability," Royal United Services Institute, 17 June 2026, https://www.rusi.org/explore-our-research/publications/commentary/checkmate-russian-orbital-manoeuvring-threatens-ukraines-space-capability.
15. Jonas Vidhammer Berge, "Ground control to Elon Musk: Stability implications of satellite mega-constellations," *European Journal of International Security*, (2026):1–19, https://doi.org/10.1017/eis.2026.10047.

16. Shizuka Kuramitsu, "UN Reaffirms Outer Space Treaty," December 2024, https://www.armscontrol.org/act/2024-12/news/un-reaffirms-outer-space-treaty.
17. For simulations regarding the cumulative radiation doses acquired by satellites over extended periods within dynamically evolving radiation belts, see the two key DTRA studies: Defense Threat Reduction Agency, Advanced Systems and Concepts Office, John Parmentola et al., "High Altitude Nuclear Detonations (HAND) Against Low Earth Orbit Satellites ('HALEOS')," April, 2001, https://spp.fas.org/military/program/asat/haleos.pdf; Conrad et al., "Collateral Damage to Satellites from an EMP Attack," 2010, 73–110, https://archive.org/details/DTIC_ADA531197.
18. Don Snyder et al., "The Effects of High-Altitude Nuclear Explosions on Non-Military Satellites," *RAND Corporation*, RRA3028-3, 3 March 2025, https://www.rand.org/pubs/research_reports/RRA3028-3.html.
19. Generally, upsets in volatile memory are resolved within milliseconds via hardware-level error detection and correction (EDAC) codes. If occurring in CPU core registers or the program counter (PC), a watchdog timer (WDT) triggers an onboard computer warm boot in less than 10 seconds. If a warm boot is insufficient, a cold boot, by removing and reapplying power, takes under a minute. Regarding hardware mitigation, see Uros Legat, Anton Biasizzo, and Franc Novak, "SEU Recovery Mechanism for SRAM-Based FPGAs," *IEEE Transactions on Nuclear Science* 59 (2012): 1142–1149. For timings of warm boot induced by the Watchdog Timer and cold boot, see Airbus Defence and Space, "AOCS/GNC Autonomy & FDIR - Challenges and way forward," (paper presented at 13th ESA Workshop on Avionics, Data, Control and Software Systems (ADCSS2019), ESA/ESTEC, Noordwijk, Netherlands, 12–14 November 2019), 5, https://indico.esa.int/event/323/contributions/5059/attachments/3761/5218/13.40_-AOCS_GNC_Autonomy_and_FDIR-_Airbus_challenges_and_way_forward.pdf.
20. This threshold was established through an exhaustive analysis of documented interaction mechanisms, drawing primarily upon the work of: Conrad et al., "Collateral Damage to Satellites from an EMP Attack," 2010; Samuel Glasstone and J. Philips Dolan, *The Effects of Nuclear Weapons* (Washington, DC: U.S. Department of Defense and Department of Energy, 1977); as well as a series of technical reports from: Carl E. Baum, "Theoretical Notes (EMP-2)," University of New Mexico, 11 October 2024, https://summa.unm.edu/notes/Theoretical.html#gsc.tab=0. Detailed derivations and the underlying physical framework are provided in Appendix B.
21. Samson et al., "FAQ: What We Know About Russia's Alleged Nuclear Anti-Satellite Weapon."
22. Glasstone and Dolan, *The Effects of Nuclear Weapons*, 518–519.
23. Snyder et al., "The Effects of High-Altitude Nuclear Explosions on Non-Military Satellites," 6.
24. Edward Savage et al., "The Early-Time (E1) High-Altitude Electro Magnetic Pulse (HEMP) and its Impact on the U.S. Power Grid," *Metatech Corporation*, Meta-R-320, January 2010, http://large.stanford.edu/courses/2019/ph241/rogers1/docs/meta-r-320.pdf.
25. Glasstone and Dolan, The Effects of Nuclear Weapons, 276.
26. Ibid.
27. Ibid., 325.
28. Snyder et al., "The Effects of High-Altitude Nuclear Explosions on Non-Military Satellites," 10-12.
29. John M. Alexander and M. Frances Gazdik, "Recoil Properties of Fission Products," *Physical Review* 120 (1960): 878.
30. Conrad et al., "Collateral Damage to Satellites from an EMP Attack," 42.

31. Ibid., 47–62.
32. Ibid., 47–50.
33. Data from CelesTrak, "NORAD GP Element Sets Current Data"; and Space-Track, "Satellite Catalog," 2025, https://www.space-track.org/basicspacedata/query/class/satcat/format/csv.
34. The European Space Agency, "Low Earth orbit," 2 March 2020, https://www.esa.int/ESA_Multimedia/Images/2020/03/Low_Earth_orbit.
35. Carey Sublette, "Operation Dominic," *The Nuclear Weapon Archive*, 27 June 202, https://nuclearweaponarchive.org/Usa/Tests/Dominic.html.
36. Data from Center for Strategic and International Studies, "Missiles of the World: Information on strike capabilities from around the globe," *MISSILETHREAT: CSIS Missile Defense Project*, 2025, https://missilethreat.csis.org/missile/; and Missile Defense Advocacy Alliance, "Missile Threat and Proliferation," 2025, https://missiledefenseadvocacy.org/missile-threat-and-proliferation/.
37. David Wright, Laura Grego, and Lisbeth Gronlund, *The Physics of Space Security: A Reference Manual* (Cambridge, MA: American Academy of Arts and Sciences, 2005), 77.
38. Carey Sublette, "The B83 (Mk-83) Bomb," *The Nuclear Weapon Archive*, 11 November 1997: https://nuclearweaponarchive.org/Usa/Weapons/B83.html.
39. Hans M. Kristensen et al. "Chinese nuclear weapons, 2025," *Bulletin of the Atomic Scientists* 81 (2025): 135–160.
40. CelesTrak, "NORAD GP Element Sets Current Data," and Space-Track, "Satellite Catalog."
41. Nehal Malik, "Starlink Reaches 7 million Users Worldwide, Expands to 150 Countries," *Tesla North*, 28 August 2025, https://teslanorth.com/2025/08/28/starlink-hits-7-million-users-worldwide-expands-to-150-countries/.
42. Jonathan McDowell, "Starlink Statistics," Jonathan's Space Pages, 31 October 2025, https://planet4589.org/space/con/star/stats.html.
43. Data from Federal Communications Commission, "In the Matter of Space Exploration Holdings, LLC: Request for Modification of the Authorization for the SpaceX NGSO Satellite System. Order and Authorization and Order on Reconsideration," FCC-21-48, 23 April 2021, 3–4, https://docs.fcc.gov/public/attachments/fcc-21-48a1.pdf; "In the Matter of Space Exploration Holdings, LLC – Request for Orbital Deployment and Operating Authority for the SpaceX Gen2 NGSO Satellite System: Order and Authorization," FCC-22-91, 29 November 2022, 7–8, https://docs.fcc.gov/public/attachments/FCC-22-91A1.pdf.
44. The European Space Agency, "PlanetScope and SkySat - The high-resolution nanosatellite constellation," 20 April 2022, https://earth.esa.int/eogateway/news/planetscope-and-skysat-infographic.
45. Jeff Foust, "Planet announces new line of satellites for daily Earth imaging," *Space News*, 10 October, 2025, https://spacenews.com/planet-announces-new-line-of-satellites-for-daily-earth-imaging/.
46. This estimation is derived from the assumption that all LEO satellites are uniformly distributed and is obtained by simply dividing the volume of the explosion range by the volume of the LEO space. See Snyder et al., "The Effects of High-Altitude Nuclear Explosions on Non-Military Satellites," 23.
47. Numbers are from Andrew Jones, "China ramps up satellite production capacity amid constellation ambitions," *Space News*, 20 April 2026, https://spacenews.com/china-ramps-up-satellite-production-capacity-amid-constellation-ambitions/; and Kuiper Systems LLC, "Application for Authority to Launch and Operate a Non-Geostationary Satellite Orbit System," FCC, ICFS File No. SAT-LOA-20260601-00224, filed

24 July 2026, https://fccprod.servicenowservices.com/icfs?id=ibfs_application_summary&number=SAT-LOA-20260601-00224.

48. Scott Pence and Adam F. Reynolds, "High-Altitude Nuclear Explosions: Myths and Reality," Center for Strategic and International Studies, 14 July 2025, https://www.csis.org/analysis/high-altitude-nuclear-explosions-myths-and-reality.
49. Sarah Scoles, "How the Government Controls Sensitive Satellite Data," *WIRED*, 8 February 2018, https://www.wired.com/story/how-the-government-controls-sensitive-satellite-data/.
50. It should be noted that China is rapidly developing its own mega-constellations, such as Xingwang and Qianfan, totaling approximately 28,000 satellites. This will significantly increase its domestic space assets, particularly at low-to-mid inclinations; for instance, the Xingwang project alone plans to deploy 12,992 satellites within the 30° to 60° range. This trend will increase the vulnerability of Chinese space assets but is also likely to mitigate the current uneven orbital distribution among nations, thereby reducing the existing vulnerability imbalance. Data from: Andrew Jones, "China ramps up satellite production capacity amid constellation ambitions"; and Yun Xu et al., "Self-Organizing Control of Mega Constellations for Continuous Earth Observation." *Remote Sensing* 14 (2022): 5896.
51. However, for states with advanced satellite manufacturing technology and launch capabilities, it may be possible to mitigate this issue by replenishing the affected systems with hardened satellites, restoring some of the space capabilities.
52. Jonathan Novak, "Policy and Design Courses of Action to Improve Resilience of Proliferated Low Earth Orbit Constellations Against Adverse Solar Weather" (master's thesis, Massachusetts Institute of Technology, 2022), 143.
53. Igor Morić, "Capabilities of Commercial Satellite Earth Observation Systems and Applications for Nuclear Verification and Monitoring," *Science & Global Security* 30 (2022): 22–49.
54. Zhengqing Fang et al., "On Lyapunov stability of artificial potential function-based low-thrust constellation reconfiguration control," *Advances in Space Research* 74 (2024): 2316–2330.
55. Zheng Li, "Jamming and Unjamming Starlink: High-Stakes Tech War in The Silent Sky," *Medium*, 15 January 2026, https://medium.com/the-low-end-disruptor/jamming-and-unjamming-starlink-high-stakes-tech-war-in-the-silent-sky-ff671e8cadfb.
56. Daniel Filipe Amaro Monteiro, "Resilience analysis of satellite internet constellations" (master's thesis, Universidade do Porto, 2023), 47.
57. ESA, "Around 100,000 satellites are expected to be in orbit by 2030."
58. Nuclear Threat Initiative (NTI), "PAROS Treaty," 27 August 2025, https://www.nti.org/education-center/treaties-and-regimes/proposed-prevention-arms-race-space-paros-treaty/.
59. Regarding on-orbit inspections, a recent study indicated that a CubeSat platform can verify a satellite's compliance with the OST on-orbit by observing the neutrons induced by spallation from the GeV protons in the inner Van Allen radiation belts to detect onboard thermonuclear weapons. See Areg Danagoulian, "Verification of the Outer Space Treaty with cosmic protons," *Nature* 655 (2026): 585–590.
60. Under the PAROS framework, since 2008, China and Russia have been forwarding the draft "Treaty on Prevention of the Placement of Weapons in Outer Space and of the Threat or Use of Force Against Outer Space Objects" (PPWT) to the United Nations Conference on Disarmament. The core obligation of the treaty requires that States Parties undertake not to place objects in orbit carrying any kind of weapons. The United States has objected to the proposal on grounds of ambiguous definitions,

verification and implementation challenges and concerns over banning ASAT systems. See: United Nations Conference on Disarmament, "Treaty on Prevention of the Placement of Weapons in Outer Space and of the Threat or Use of Force against Outer Space Objects (PPWT)," CD/1839, 29 February 2008; "Russian Federation and China: Updated Text of PPWT," CD/1985, 12 June 2014; and "United States of America: Analysis of the 2014 Russian-Chinese Draft Treaty on the Prevention of the Placement of Weapons in Outer Space, the Threat or Use of Force against Outer Space Objects," CD/1998, 3 September 2014.

61. Parmentola et al., "High Altitude Nuclear Detonations," 15–16.
62. The number of Starlink satellites launched per week from Michael Kan, "SpaceX Offers Rare Peek Inside a Starlink Satellite Factory, Tips 'Mini Lasers'," *PCMag*, 27 August 2025, https://au.pcmag.com/networking/112769/spacex-offers-rare-peek-inside-a-starlink-satellite-factory-tips-mini-lasers; The number of satellites launched globally each year from BryceTech, "Global Space Launch Activity in 2024," https://brycetech.com/reports/report-documents/global-space-launch-activity-2024/.
63. William Atwell et al., "Mitigating the effects of the space radiation environment: a novel approach of using graded-z materials," AIAA Paper 2013–5385, (paper presented at AIAA SPACE 2013 conference and exposition, San Diego, California, U.S., 10–12 September 2013), 1–10.
64. Piero Spillantini, "Shielding from cosmic radiation for interplanetary missions: Active and passive methods," *Radiation Measurements* 42 (2007): 14–23.
65. Precedence Research, "Radiat
66. AMPLYFi, "Understanding the Space Debris Dilemma: The Kessler Syndrome," 16 June 2025, https://amplyfi.com/blog/understanding-the-space-debris-dilemma-the-kessler-syndrome/.
67. Jakub Drmola and Tomas Hubik, "Kessler Syndrome: System Dynamics Model," *Space Policy* 44 (2018): 29–39.
68. The European Space Agency, Space Debris Office, "ESA Space Environment Report 2025," 1 April 2025, https://www.esa.int/Space_Safety/Space_Debris/ESA_Space_Environment_Report_2025.
69. Drmola and Hubik, "Kessler Syndrome: System Dynamics Model."
70. Boley and Byers, "Anti-satellite weapon tests to disrupt large satellite constellations."

Acknowledgments

This work was funded in part through grants by the Andrew Carnegie Foundation to the Program on Science and Global Security.

Disclosure statement

The authors declare that they have no known competing financial interests or personal relationships that could have appeared to influence the work reported in this paper.

Data availability statement

Data will be made available on request.

Appendix A: Delayed effects of HANE

Long-term radiation

Free electrons resulting from HANE will be trapped in artificial radiation belts for extended periods due to the Earth's magnetic field, creating a hostile environment which can persist for years, decreasing the lifespans of passing satellites. The 2001 DTRA report analysis of a 20-kt HANE at 290 km demonstrated that unshielded satellites at 800–1400 km would fail within 10–60 days. The radiation would decay to normal levels within 6 to 24 months.[61] In general, the extent and duration of risk depend on where the trapped electrons would be concentrated and the degree of satellite hardening. Given the rapidly expanding global launch capacity, the affected satellites can be rapidly replenished after the radiation belts have completely cooled. Considering the high-throughput production capabilities (e.g., Starlink at 70 units/week) and the current launch rate of 3,000 satellites per year, restoring from zero to the current level of 12,000 satellites only takes 4 years.[62] Furthermore, passive materials such as polyethylene, aluminum, and composites can provide radiation shielding.[63] Active electromagnetic fields offer another form of protection.[64] Process- and design-level hardening, including silicon-on-insulator (SOI) and triple modular

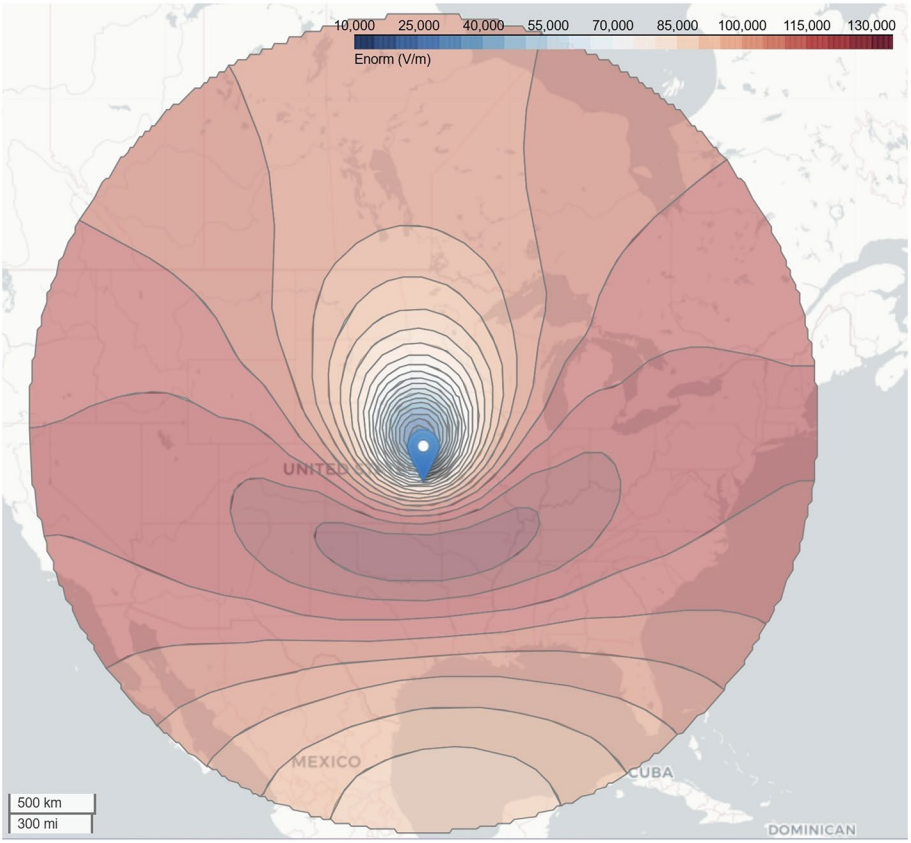


Figure A1. Contour plot of the maximum EMP intensity for $Y = 1$ Mt nuclear detonation 400 km directly overhead topeka, Kansas, USA (95.675°W, 39.050°N) within the line of sight. The figure was generated using the open-source code provided by Hartnett.

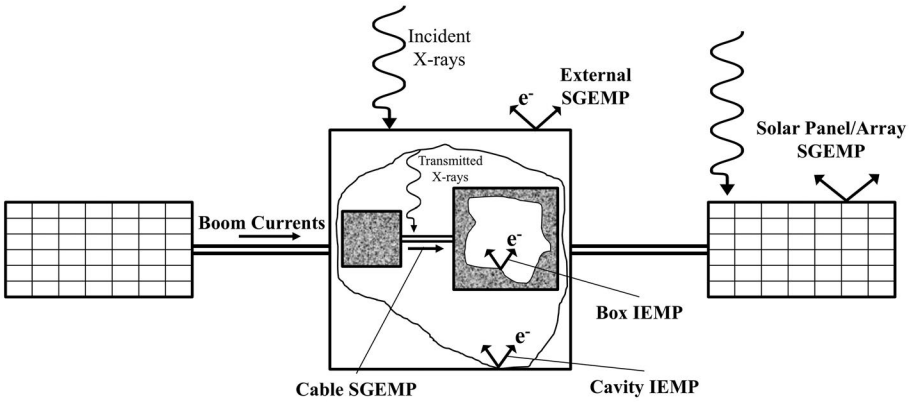


Figure A2. Basic SGEMP processes for a satellite.

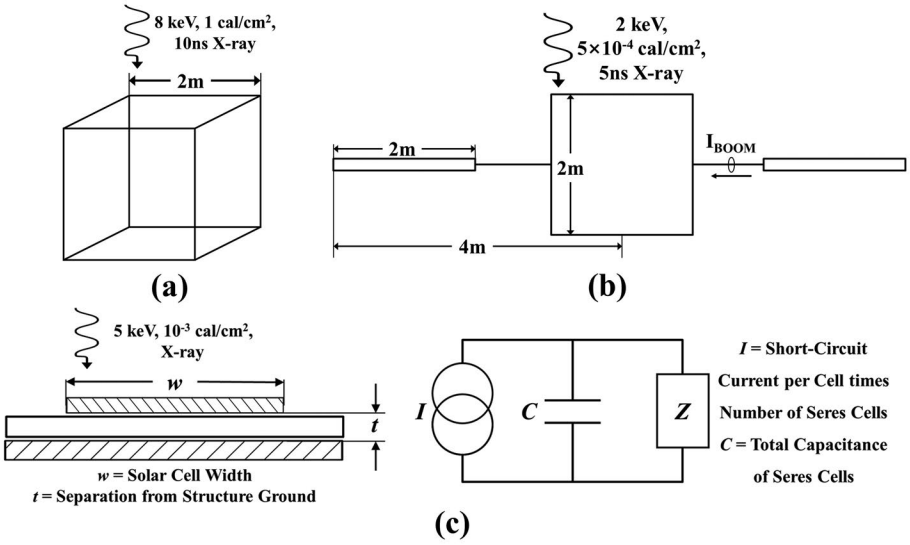


Figure A3. Three scenarios of external SGEMP: body current (a), boom current (b), and solar cells coupling current with equivalent circuit (c).

redundancy (TMR), can further improve resilience.[65] Together, these measures may reduce the required radiation cooling time.

Chain reaction of space debris collisions: the Kessler Syndrome

Another common concern is HANE's potential to trigger the Kessler Syndrome, a self-perpetuating cascade of space-debris collisions, whereby increasing object density in LEO generates additional debris, which in turn increases the probability of further impacts, and ultimately makes LEO unusable for satellite operations and launches.[66]

In fact, HANE generates debris only in a limited region, since satellites disabled by SGEMP remain intact and would not disintegrate immediately. Debris mainly originates from warhead fragmentation and thermomechanical breakup of satellites, which only occurs within 20–200 km of the detonation point, estimated from Equation (1). According to

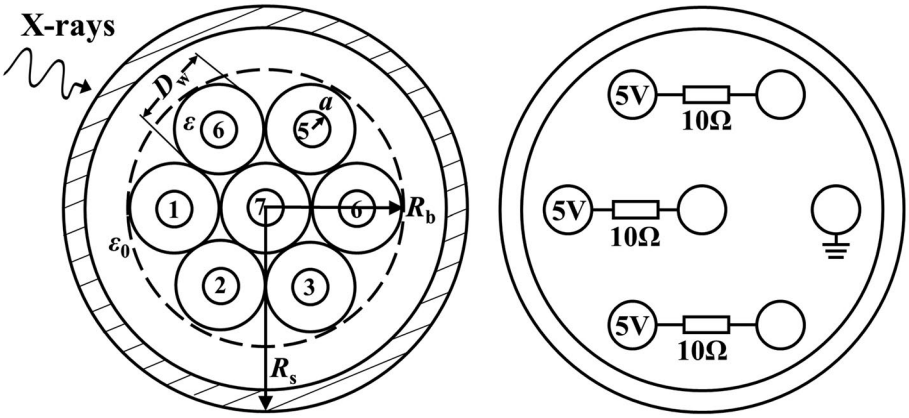


Figure A4. A bundle of seven identical insulated wires of radius a within a metal shield (left) and loads configuration (right).

Drmola and Hubik, space debris growth from a single Starfish Prime-level HANE is roughly consistent with that from current launch rates in peaceful environment.[67] Thus, the collision probability is similar, estimated by ESA's annual space environment report at fewer than 10 per year over the next two centuries.[68] In addition, such collisions can even be largely avoided, as tracking and evading inactive satellites is a simpler task than with small fragments.[69] Therefore, given the long timescale between collisions, using a HANE to trigger a destructive debris-collision cascade provides no immediate military advantage, and concerns about such chain reactions can be set aside.[70]

Ground electromagnetic pulse (EMP)

Gamma rays from a HANE strike molecules in the atmosphere, producing large numbers of free electrons that are accelerated by Earth's magnetic field into intense, rapidly changing currents, which in turn generate a ground-level EMP. This EMP could affect satellites indirectly by damaging their ground support systems or ground systems that use the satellites' services. Among the three components of ground-level EMP, E1, a nanosecond, high-voltage, high-frequency early-time pulse, is the primary cause of electronic-system damage.

To quantify the spatial extent of ground EMP effects, a map of EMP intensity over the circular region of ground points within line of sight of the burst using the Karzas–Latter–Seiler model was generated, as shown in Figure A1. The characteristic "smile" pattern shows comparatively weak fields at ground zero, weaker still directly north, and much stronger fields in a half-annular region immediately south. The maximum EMP intensity at ground zero increases with the yield Y but decreases with the HOB. When Y reaches 1 Mt, the intensity can reach up to 10^5 V/m.

However, for the ground systems of critical satellites, EMP effects can be mitigated by remote or mobile sensitive compartmented information facilities, relocated command-and-control systems, shielded electronic equipment, and backup batteries or generators.

On the other hand, HANE ionizes the upper atmosphere, sharply increasing ionospheric electron density over regions that can extend thousands of kilometers beyond the burst's line of sight, thereby disturbing the ionospheric structure, causing absorption, refraction,

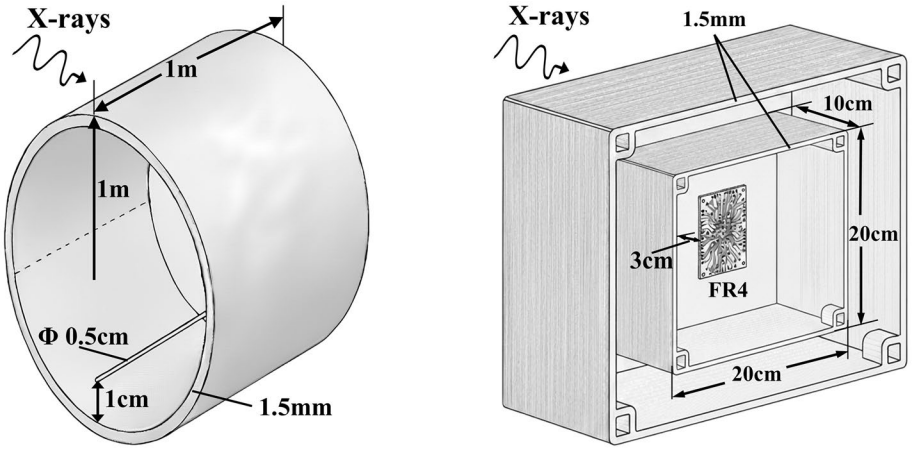


Figure A5. Schematic diagram of Cavity IEMP (a) and Box IEMP simulation scenario (b).

Table A1. SGEMP definition, categories and their failure threshold (upset/burnout).

		Failure Threshold (cal/cm^2)	
SGEMP Category	Definition	Upset	Burnout
External SGEMP	Occurs on the exterior surface of the platform, due to reverse pC electron emission from surface materials.	—	5.5×10^{-3}
Cable SGEMP	Occurs within system cabling harnesses, often dominated by electron emission from interior surface of the cable shield.	—	0.5
Cavity IEMP	Occurs within cavities of the platform, usually dominated by electron emission from the cavity walls.	3×10^{-4}	0.01
Box IEMP	Occurs within electronics boxes, often dominated by electron emission from the circuit board traces and connecting conductors.	0.2 (3 keV Uncoated) 0.005 (7 keV Uncoated) 0.2 (3 keV Coated) 0.2 (7 keV Coated)	10 (3 keV Uncoated) 0.2 (7 keV Uncoated) 100 (3 keV Coated) 10 (7 keV Coated)

scattering, phase anomalies, and Doppler shifts of radio signals passing through, thereby disrupting radio communications, radar, and related systems.

Nevertheless, the dominant effect is confined to medium and high-frequency (MF/HF) systems and lasts only a few hours up to one day, with secondary impacts on low-frequency (LF) and very-high-frequency (VHF) and minimal effects on ultra-high-frequency (UHF). The affected area increases with both HOB and yield, while the disturbance duration decreases as HOB increases. Generally, LEO satellites use VHF and UHF bands for ground-based telemetry, tracking, and command (TTC), whereas communication and navigation satellites employ L, S, C, X, Ku, K, Ka, and related bands (about 1–40 GHz) for

Table A2. Starlink configuration parameters.

	Altitude (km)	Inclination i (°)	Orbital Planes (P)	Sat Per Plane	Total Satellites (T)
Starlink Gen1	550	53	72	22	1584
4,408	540	53.2	72	22	1584
	570	70	36	20	720
	560	97.6	6	58	348
	560	97.6	4	43	172
Starlink Gen2	340	53	48	110	5280
29,988	345	46	8	110	5280
	350	38	48	110	5280
	360	96.9	30	120	3600
	525	53	28	120	3360
	530	43	28	120	3360
	535	33	28	120	3360
	604	148	12	12	144
	614	115.7	18	18	324

Table A3. Planet constellation configuration parameters (At 2022-03-01 T00:00:00Z).

		Altitude	Inclination	Total Satellites
	PlanetScope 354 Flock/Doves	475 km-525 km SSO	97°–98°	354
21 SkySats	SkySat-1-2	600 km SSO	97°–98°	2
	SkySat-3-15	500 km SSO		13
	SkySat-16-21	450 km non-SSO	53°	6

ground links. Even if communication is affected, data could be routed via inter-satellite links and ground-based non-radio channels (e.g., fiber-optic networks), so ground-level EMP from a HANE would have a minimal effect on satellite–ground communication.

Appendix B: Calculation process for the thresholds of thermal, SGEMP and ionizing induced failure

Thermal effects

When X-rays are absorbed, part of their energy is converted to heat, raising the temperature of exposed surfaces. If absorbed fast enough, this energy can cause melting, spallation, or create a shock wave causing fractures, damaging materials throughout the satellite. Solar panels, the primary power source on most satellites, are particularly susceptible to these thermal effects. The thermal impact on components depends on the X-ray spectrum, deposition time profile, and the thermal, mechanical, and atomic (Z) properties of the absorbing material. A conservative estimate of surface damage, neglecting thermal diffusion, is obtained by dividing the surface dose by the material specific heat.

For 1 keV blackbody radiation, surface melting typically requires >0.2 cal/cm^2 for low-Z materials but <0.1 cal/cm^2 for high-Z materials (1 cal/cm^2 $\approx$ 4.184×10^4 J/m^2). In satellites, low-Z materials are mainly structural metals and composites such as aluminum (Al), titanium (Ti), and carbon-fiber–reinforced polymer (CFRP), whereas high-Z materials are dense metals such as tungsten (W), gold (Au), and lead (Pb).

SGEMP effects

When a system is exposed to X-rays, photo-Compton electron currents are emitted from the various surfaces and driven throughout surrounding materials. The resulting currents

generate transient electromagnetic fields within the system, which in turn induce currents and voltages on various components, a phenomenon known as SGEMP.

These induced signals can be coupled into electronic devices and cause upset or burnout, potentially leading to mission failure. Here, upset denotes a temporary, undesired change of logic state in a digital circuit, whereas burnout is a permanent failure from irreversible damage due to excessive overcurrent or overvoltage.

Figure A2 illustrates the basic SGEMP process, which is commonly classified into four types: external SGEMP, cable SGEMP, cavity IEMP, and box IEMP. A brief explanation of these SGEMP categories is provided in Table A1. In the presented analysis, a nominal upset threshold of 5 V and a burnout criterion of 1μJ absorbed energy were adopted. The corresponding X-ray fluence thresholds for upset and burnout for each SGEMP category are listed in the last two columns of Table A1, with calculation details provided under "External SGEMP," "Cable SGEMP," "Cavity IEMP," and "Box IEMP."

External SGEMP

External SGEMP can occur on the satellite body surface, booms, and solar panels/arrays. Relevant studies have been presented in multiple papers.

The satellite body current caused by external SGEMP is shown in Figure A3(a). For a satellite with a 2 m cubic central body exposed to 1 cal/cm^2 of 8-keV X-rays with a 10 ns pulse, the peak body replacement current is 1,900 A with a bandwidth of about 18 ns. The boom current caused by external SGEMP is shown in Figure A3(b), for a satellite with a 2 m cubic central body, two 3 m × 2 m solar panels, and a boom of length $l = 2$ m, exposed to 5×10^{-4} cal/cm^2 of 2-keV X-rays with a 5 ns pulse width. Simulation results indicate that the boom current exhibits a normal damped sinusoidal behavior, with a peak of 200 mA, decaying to 15–20% of its prompt peak within 200 ns. These examples indicate that external SGEMP primarily affects metallic structures rather than electronic components. However, body currents may also couple to wires within the satellite Faraday cage both diffusively and through apertures and seams in the cage, or couple inductively to wires and wire shields outside the Faraday cage. In many satellites, the solar array boom penetrates the Faraday cage, allowing direct current coupling to internal wires and shields.

The external SGEMP coupling to satellite solar cells is illustrated in Figure A3(c). A 10 Ω load represents the direct drive between a string of 100 solar cells and structural ground. Each 6.5 cm × 6.5 cm cell is separated from the substrate by a 0.25 mm dielectric with permittivity $3\varepsilon_0$ The array is exposed to 10^{-3} cal/cm^2 of 5-keV X-rays, producing a load current of 86 mA with a decay time of 460 ns. Assuming the current scales linearly with the X-ray fluence and using $E = I^2Rt$ with a burnout threshold of 1 μJ, the induced current is 466 mA, corresponding to an X-ray fluence of 5.5×10^{-3} cal/cm^2.

Cable SGEMP

A set of theoretical notes issued by the Air Force Weapons Laboratory (AFWL) provides a method for calculating the Cable SGEMP response. The simulation model, shown as Figure A4, utilized a bundle of seven identical insulated wires with an outer 1.27 mm Al shield, which provides a vacuum gap between the effective outer radius of the bundle R_b=1 cm and the shield radius R_s=1.2 cm. Each wire had a radius of $a = 0.25$ cm and was insulated with 0.08 cm polyethylene ($\varepsilon = 2.3\varepsilon_0$). The conductors were 1 m copper wires with loads R_L=10 Ω. The simulation assumed a 5 keV X-ray fluence of 0.1 cal/cm^2 incident at 30°. Simulation results show that the peak differential voltage between wires was 2.16 V and scaled linearly

with fluence. For an EMP duration $t \approx 100\,\text{ns}$, using $E = I^2 R_L t$ with a burnout threshold of 1 μJ gives an induced current of 1 A, corresponding to a differential voltage of about 10 V, i.e., five times the simulated value. Thus, burnout in this configuration requires an X-ray fluence of approximately $0.5\,\text{cal/cm}^2$.

Cavity IEMP

To investigate the effect of Cavity IEMP on internal satellite components, the 2010 DTRA report performed a simulation using the Testable Hardware Toolkit V2.0. The scenario, shown as Figure A5(a), modeled a cylindrical body (1 m radius × 1 m length) with a 1.5 mm Al wall and an empty cavity. Inside, a bare Al wire (0.5 cm diameter, 100 cm length) was positioned 1 cm above the wall/ground plane. Adopting thresholds of 5 V for upset and 1 m radius × 1 m length, the simulation results indicate that a 3 keV X-ray source requires approximately $3 \times 10^{-4}\,\text{cal/cm}^2$ of fluence to trigger upset and $10^{-2}\,\text{cal/cm}^2$ to cause burnout.

Box IEMP

To estimate the severity of Box IEMP effects, the 2010 DTRA report analyzed a 20 cm × 20 cm × 10 cm uncoated Al enclosure with 1.5 mm walls, shown as Figure A5(b). A 0.8 mm circuit board with a single bottom copper ground plane was placed 3 cm from one wall. The board contained circuit traces which were 0.25 mm wide by 40 cm long, consisting of 35 μm thick copper and 76 μm solder connections.

Two hardness levels were considered: a hardened board with a 76 μm polyurethane conformal coating and a bare board with all metal exposed. The damage thresholds were the same as Cavity IEMP, but now the X-ray must traverse 1.5 mm Al cavity and the 1.5 mm box wall. The simulation considered scenarios at 7 keV and 3 keV of X-ray. For the uncoated circuit board, burnout occurs at a minimum 3 keV X-ray fluence of $0.2\,\text{cal/cm}^2$. The X-ray fluences required for upset and burnout under the other conditions are summarized in the bottom row of Table A1.

Ionizing effects

Higher-energy X-rays can ionize materials, to which semiconductor devices are particularly sensitive. Ionization can temporarily upset or permanently damage electronics and electronic memory. The analysis of ionizing effects originates from the study of Transient Radiation Effects on Electronics (TREE). Based on the radiation interaction mechanism, the response of electronics is divided into total-dose effects and dose rate effects.

Dose rate effects

HANE-generated transient X-ray bursts ionize electronic materials and generate internal fields. The induced currents can discharge capacitors, make cable insulation conductive, and switch on reverse-biased junctions, causing logic errors and memory loss. Such damage caused by the Dose-rate effects are generally classified as upset or latch-up. Upset is an event that produces an unwanted change of logic state in a digital circuit. In some instances, the circuit can restore the proper logic state by itself. This occurs when dose rate reaches $10^6\,\text{rad/s}$, response to an X-ray fluence of $10^{-6}\,\text{cal/cm}^2$. Latch-up is an event that creates

a low-impedance path, causing a high-current flow and potentially leading to permanent device failure. It can be observed when dose rate reaches 10^8~10^{10} rad/s, response to an X-ray 10^{-3}~10^{-2} cal/cm^2.

Total dose effects

Total ionizing dose (TID) is the most common form of radiation damage in satellite electronics. With continued exposure, radiation-generated electron–hole pairs drift under the electric field and become trapped in insulating layers and at semiconductor–insulator interfaces. The resulting charge buildup creates internal fields that shift transistor threshold voltages, causing degraded switching and increased power consumption.

Once the absorbed dose exceeds a critical level, this degradation can lead to device failure. To quantify damage, the X-ray dose absorbed by the satellite during a HANE event is evaluated. For a satellite with area-to-mass ratio S/m, the absorbed ionizing dose D is:

$$D = \frac{F_{\text{x-ray}} S}{m} (\text{rad}) \tag{A1}$$

The satellite area-to-mass ratio is typically 0.01 to 0.1 m^2/kg. LEO satellites below 800 km with 3-to-5-year lifetimes can usually tolerate about 3–5 krad. Here the hardening was assumed to be twice the average natural background and TID threshold of 10 krad was adopted. Substituting these values into Equation (A1) yields satellite failure from total ionizing dose at an X-ray fluence of 10^2 to 10^3 J/m^2.

Appendix C: Orbital dynamics and constellation configuration

This appendix outlines the methodology for calculating the constellation configuration and the orbital position of each satellite based on measured data or design intent.

As the TLE epochs T_e are non-uniform across the satellites retrieved from CelesTrak, all positions are propagated to a common epoch T_p using a simplified two-body model, where the semi-major axis a, eccentricity e, inclination i, RAAN , and argument of perigee ω are held constant at their TLE-acquired values; The mean anomaly M_p at epoch T_p is calculated as:

$$M_p = M_{\text{TLE}} + n_{\text{TLE}} (T_p - T_e) \tag{A2}$$

where M_{TLE} and n_{TLE} are the mean anomaly and mean motion extracted from the TLE at epoch T_e.

The configuration of the proposed completed Starlink constellation, with a total of 34,396 satellites (including 4,408 Gen1 and 29,988 Gen2 satellites) as given in Table A2. It is assumed that each layer adopts a Walker-Delta configuration, often denoted by the notation i: $T/P/F$. This is a symmetric configuration where T satellites are distributed equally across P orbital planes, all sharing the same inclination i and altitude. The planes are uniformly spaced in Right Ascension of the Ascending Node (RAAN), and the phasing factor F defines the relative angular separation (true anomaly) of satellites between adjacent planes. Without loss of generality, the RAAN Ω and true anomaly f of the k-th satellite in the j-th orbital plane satisfy the following conditions:

$$\Omega^{(j,k)} = \frac{360^\circ}{P} \times (j - 1) \tag{A3}$$

$$f^{(j,k)} = \frac{360°}{T} \times \left[P\left(k-1\right) + F\left(j-1\right) \right] \tag{A4}$$

Through the data in Equations (A3) and (A4), and Table A2, the orbital elements for all Starlink satellites can be obtained, thereby determining their three-dimensional positions.

For the Planet constellation, it does not adhere to the Walker-Delta configuration. Therefore, CelesTrak was searched for Flock and SkySat satellites to obtain their NORAD IDs. These IDs were then cross-referenced with historical data queried from the Space-Track website to retrieve their orbital elements. PlanetScope satellites are mainly in SSO at 475 km–525 km altitude with inclinations of 97°–98°. Among the 21 SkySat satellites, SkySat-1 to 15 are also in SSO with inclinations of 97°–98°; specifically, SkySat-1 and 2 are at approximately 600 km, and SkySat-3 to 15 were at 500 km at launch, lowered to 450 km in early 2020. In contrast, SkySat-16 to 21 are in inclined, non-SSO orbits at approximately 400 km with a 53° inclination. The details are shown in Table A3.